Scientific and Educational Reports of the Faculty
of Science and Technology, Kochi University
Vol. 1 (2018), No. 2

How nuclear incompressibility affects shell structure of superheavy nuclei

Kei Iida,[1, 2, *] Mari Adachi,[2] and Kazuhiro Oyamatsu[3]

[1] *Department of Mathematics and Physics, Kochi University, Kochi 780-8520, Japan*
[2] *Department of Natural Science, Kochi University, Kochi 780-8520, Japan*
[3] *Department of Human Informatics, Aichi Shukutoku University, 9 Katahira, Nagakute, Aichi 480-1197, Japan*

We systematically examine how the structure of superheavy nuclei depends on the equation of state of nuclear matter. In doing so, we first describe the neutron and proton distributions of such nuclei within a simplified Thomas-Fermi framework in such a way as to reproduce empirical masses and charge radii of stable nuclei. We then calculate the central and Coulomb parts of the single-particle potential, which are complemented by the spin-orbit part that makes the resultant single-particle spectra for ^{208}Pb consistent with the empirical behavior. We find that the incompressibility of symmetric nuclear matter significantly affects the calculated $Z = 28$, 50, 82 gaps for ^{278}113 and ^{294}118.

Recent experiments to synthesize superheavy nuclei not only produced several new elements, but also led to implications for the island of stability on the chart of nuclides [1]. Even in relatively lighter nuclides such as ^{208}Pb, however, it is poorly known how the single-particle levels look like well below the Fermi energy. This is related to uncertainties in the spin-orbit part of the single-particle potential, which scales as the gradient of the nuclear density distribution. This distribution is in turn connected with the equation of state (EOS) of nuclear matter in a way clearer for heavier nuclei [2]. It is thus important to ask the question of how the EOS of nuclear matter affects the internal shell structure of heavy and superheavy nuclei through the spin-orbit potential.

So far, the EOS of nuclear matter has yet to be well determined even at subnuclear densities [3]. Empirical data such as nuclear masses and radii are not sufficient to severely constrain the EOS, while many-body calculations depend on what kind of nuclear forces and approximate procedures are adopted even in the simple case of pure neutron matter. We thus start with model EOSs that account for possible uncertainties. In previous works [2, 4, 5], two of the present authors address the questions of how such EOSs affect the macroscopic prediction of radii and masses of unstable neutron-rich nuclei. In this case, the poorly known density dependence of the symmetry energy controls the radii and masses through the bulk and surface properties, respectively. In the present work, we consider the EOS effect on the single-particle levels of superheavy nuclei ^{278}113 and ^{294}118, which were synthesized in laboratories [6, 7] and recently given an element name as nihonium (Nh) and oganesson (Og), respectively.

For the purpose of clarifying such effects, we first calculate, within a simplified Thomas-Fermi model of a nucleus, the neutron and proton density distributions in a manner that is dependent on the EOS while reproducing empirical masses and charge radii of stable nuclei. From the optimal neutron and proton density distributions, we evaluate the central, Coulomb, and spin-orbit parts of the neutron and proton single-particle potentials, in which we determine the effective range of the nuclear force and the strength of the spin-orbit potential in such a way as to reproduce empirical single-particle energies of ^{208}Pb. We then solve the Schrödinger equations to obtain the neutron and proton single-particle levels of superheavy nuclei for various EOSs. In this work, for simplicity, we assume that the nuclear density distributions are spherically symmetric.

We begin by describing the total energy of a nucleus of charge number Z and neutron number N in terms of the local neutron and proton density distributions $n_n(\mathbf{r})$ and $n_p(\mathbf{r})$ by using the following energy density functional:

$$E = E_b + E_g + E_C + Nm_nc^2 + Zm_pc^2, \tag{1}$$

where

$$E_b = \int d^3r n(\mathbf{r}) w\left[n_n(\mathbf{r}), n_p(\mathbf{r})\right] \tag{2}$$

is the bulk energy with $n(\mathbf{r}) = n_n(\mathbf{r}) + n_p(\mathbf{r})$ and the energy w per nucleon of uniform nuclear matter,

$$E_g = F_0 \int d^3r |\nabla n(\mathbf{r})|^2 \tag{3}$$

is the gradient energy with adjustable constant F_0,

$$E_C = \frac{e^2}{2} \int d^3r \int d^3r' \frac{n_p(\mathbf{r}) n_p(\mathbf{r}')}{|\mathbf{r} - \mathbf{r}'|} \tag{4}$$

is the Coulomb energy, and m_n (m_p) is the neutron (proton) mass.

The bulk energy (2) dominates Eq. (1), while being controlled by the energy w of uniform nuclear matter within the framework of the local density approximation. For w, just like the previous works [2, 4, 5] based on Eq. (1), we adopt the phenomenological EOS models in the form of [8]

$$w(n_n, n_p) = \left[t(n_n, n_p) + v(n_n, n_p)\right]/n \tag{5}$$

with the kinetic energy density,

$$t = \frac{3\hbar^2(3\pi^2)^{2/3}}{10m_n}(n_n^{5/3} + n_p^{5/3}) \tag{6}$$

*Electronic address: iida@kochi-u.ac.jp

Received: January 14, 2018
Reviewed by anonymous referee, and accepted: January 27, 2018
Published: March 31, 2018

and the potential energy density,

$$v = (1-\alpha^2)v_s(n) + \alpha^2 v_n(n), \tag{7}$$

where

$$v_s = a_1 n^2 + \frac{a_2 n^3}{1+a_3 n} \tag{8}$$

and

$$v_n = b_1 n^2 + \frac{b_2 n^3}{1+b_3 n} \tag{9}$$

are the potential energy densities for symmetric nuclear matter and pure neutron matter, and $\alpha = (n_n - n_p)/n$ is the neutron excess.

It is useful to note that near the saturation point of symmetric nuclear matter, the energy per nucleon given by Eq. (5) reduces to a familiar expansion, namely [9],

$$w = w_0 + \frac{K_0}{18n_0^2}(n-n_0)^2 + \left[S_0 + \frac{L}{3n_0}(n-n_0)\right]\alpha^2. \tag{10}$$

Here w_0, n_0, and K_0 are the saturation energy, the saturation density, and the incompressibility of symmetric nuclear matter. L and S_0 are associated with the density dependent symmetry energy coefficient $S(n)$ via $S_0 = S(n_0)$ and $L = 3n_0(dS/dn)_{n=n_0}$. As the neutron excess increases from zero, the saturation point moves from (n_0, w_0) in the density versus energy plane. Up to second order in α, the saturation energy w_s and density n_s are given by

$$w_s = w_0 + S_0\alpha^2 \tag{11}$$

and

$$n_s = n_0 - \frac{3n_0 L}{K_0}\alpha^2. \tag{12}$$

The six parameters $a_1, \cdots, b_3$ are related to the EOS parameters n_0, w_0, K_0, S_0, and L. As in Refs. [2, 4, 5], we assume various sets of K_0 and L in the range of $0 < L < 160$ MeV and 180 MeV $\leq K_0 \leq$ 360 MeV, while the others are determined in such a way that the mass and charge radius of stable nuclei that can be calculated from optimization of Eq. (1) are consistent with the empirical values. We remark that the parameter b_3, which controls the EOS of matter for large neutron excess and high density while having little effect on the saturation properties of nearly symmetric nuclear matter, is set to the typical value 1.58632 fm^3, which was obtained by one of the authors [8] in such a way as to reproduce the neutron matter energy of Friedman and Pandharipande [10].

For fixed (K_0, L), we optimize Eq. (1) by assuming the nucleon distributions $n_i(r)$ $(i = n, p)$ of a nucleus of given Z and N, where r is the distance from the center of the nucleus, to be

$$n_i(r) = \begin{cases} n_i^{\rm in}\left[1 - \left(\dfrac{r}{R_i}\right)^{t_i}\right]^3, & r < R_i, \\ 0, & r \geq R_i. \end{cases} \tag{13}$$

Here, R_i roughly represents the nucleon distribution radius, t_i the relative surface diffuseness, and $n_i^{\rm in}$ the central number density. We then determine n_0, w_0, S_0, and F_0 by fitting the resultant masses and charge radii to the experimental values, which leads to about 200 sets of the EOS models as shown in Ref. [2]. Note that the present analysis can be regarded as a simplified version of the Thomas-Fermi theory, which assumes the form of $n_i(r)$ but still can well reproduce the empirical charge distribution of stable nuclei.

By building the EOS models described above into Eq. (1), we have calculated the nucleon density distributions for ^{208}Pb, ^{278}113, and ^{294}118, from which we shall calculate the single-particle energies. As clarified in Ref. [2], the results show the tendency that the central density decreases with L, while the surface diffuseness decreases with K_0. The latter feature plays a vital role in affecting the internal shell structure via the spin-orbit potential.

We now move on to the single-particle energies by constructing the single-particle potential from the optimal nucleon density distributions obtained above. We first calculate the single-particle potential $U_{0(i)}$ $(i = n, p)$ for uniform nuclear matter as

$$U_{0(i)} = \frac{\partial v(n_n, n_p)}{\partial n_i}. \tag{14}$$

By substituting the optimal distributions into Eq. (14), we obtain the central part of the single-particle potential within the local density approximation in which the range of the nuclear force is set to zero. Here, as in Ref. [11], we incorporate the finite range of the nuclear force into the potential $U_{0(i)}(r)$ via

$$U_i(r) = \left(\frac{1}{\sqrt{\pi}\kappa}\right)^3 \int d^3r' U_{0(i)}(\mathbf{r}') \exp\left(-\frac{|\mathbf{r}-\mathbf{r}'|^2}{\kappa^2}\right), \tag{15}$$

where κ is the adjustable parameter that corresponds to the range of the nuclear force. Note that in the Thomas-Fermi framework as described above, the gradient energy (3) represents the correction term due to the finite range of the nuclear force.

The Coulomb potential, which takes effect solely for protons, reads as

$$V_C(r) = \frac{\delta E_C[n_p(\mathbf{r})]}{\delta n_p(\mathbf{r})}, \tag{16}$$

where the density distributions are the optimal ones.

Finally, we set the spin-orbit part of the single-particle potential as

$$V_{\rm LS}(r) = \frac{1}{r}\left\{\lambda_1 \frac{dn(r)}{dr} \pm \lambda_2 \frac{d}{dr}\left[n_n(r) - n_p(r)\right]\right\} \mathbf{l}\cdot\mathbf{s}, \tag{17}$$

where $\mathbf{l}$ is the orbital angular momentum, $\mathbf{s}$ is the spin angular momentum, λ_1 and λ_2 are the adjustable parameters that control the strength of the isoscalar and isovector parts of the spin-orbit potential, and $\pm$ are taken for

neutrons (+) and protons (−). This part is crucial to the internal shell structure, while being sensitive to the EOS of nuclear matter, the incompressibility in particular.

We proceed to calculate the single-particle energies ε by solving the Schrödinger equations for neutrons and protons,

$$\left[-\frac{\hbar^2}{2m_n}\Delta + U_n(r) + V_{\rm LS}(r)\right]\psi(\mathbf{r}) = \varepsilon\psi(\mathbf{r}), \quad (18)$$

$$\left[-\frac{\hbar^2}{2m_p}\Delta + U_p(r) + V_C(r) + V_{\rm LS}(r)\right]\psi(\mathbf{r}) = \varepsilon\psi(\mathbf{r}). \quad (19)$$

To determine the parameters κ, λ_1, and λ_2 in such a way as to reproduce the experimental single-particle energies of ^{208}Pb near the Fermi energies, we solve Eqs. (18) and (19) for each EOS model. As a result of this fitting, the parameters κ, λ_1, and λ_2 are constrained as $\kappa = 1.15$–1.35 fm, $\lambda_1 = 170$–210 MeV fm^5, and $\lambda_2 = 10$–170 MeV fm^5.

In Fig. 1, we illustrate the EOS dependence of the single-particle energies of ^{208}Pb. Here, we adopt the five EOS models with $(K_0, L) = (180, 5.66)$, $(180, 52.2)$, $(230, 42.6)$, $(360, 12.8)$, and $(360, 146)$ in MeV; the EOS of $(230, 42.6)$ is a typical case, while the others are extreme ones. Hereafter, we refer to these five EOS sets as G, A, E, I, and C, according to Fig. 1 in Ref. [4]. The corresponding values of κ, λ_1, and λ_2 are tabulated in Table I. We can observe that the neutron and proton levels near the respective Fermi level are well constrained from the fitting for all the EOS models, while the $Z = 28, 50$ gaps decrease with K_0 to an extent in which they are no longer main gaps. We remark in passing that the neutron internal shell structure is comparatively rather insensitive to the EOS models (see Table II) and that the proton and neutron low-lying levels go up with increase in K_0. The latter reflects the fact that the kinetic energy decreases with increasing K_0, a feature related to the correlation between K_0 and n_0 that comes from fitting to empirical charge radii of stable nuclei [2].

Let us now show the results for ^{278}113 and ^{294}118. The $Z = 28, 50, 82$ gaps decrease with K_0 and, more importantly, are no longer main gaps even for the smallest K_0, as illustrated in Figs. 2 and 3 as well as in Table II. The $N = 50, 82, 126$ gaps also decrease with K_0, but remain main gaps except for the largest K_0. Such reduction in the gaps can be seen, e.g., in the previous work by Dudek [13] who used various sets of the Woods-Saxon potentials that reproduce the experimental data for the single-particle level spectra of doubly magic nuclei, although the K_0 dependence was not discussed therein.

Finally, we emphasize that the present analysis is not relevant to the prediction of the location of the stability

TABLE I: The spin-orbit and range parameters for various EOS sets.

EOS	G	A	E	I	C
K_0 (MeV)	180	180	230	360	360
L (MeV)	5.66	52.2	42.6	12.8	146
κ (fm)	1.15	1.17	1.22	1.31	1.34
λ_1 (MeV fm^5)	177	181	184	188	202
λ_2 (MeV fm^5)	10.7	20.5	28.2	34.4	138

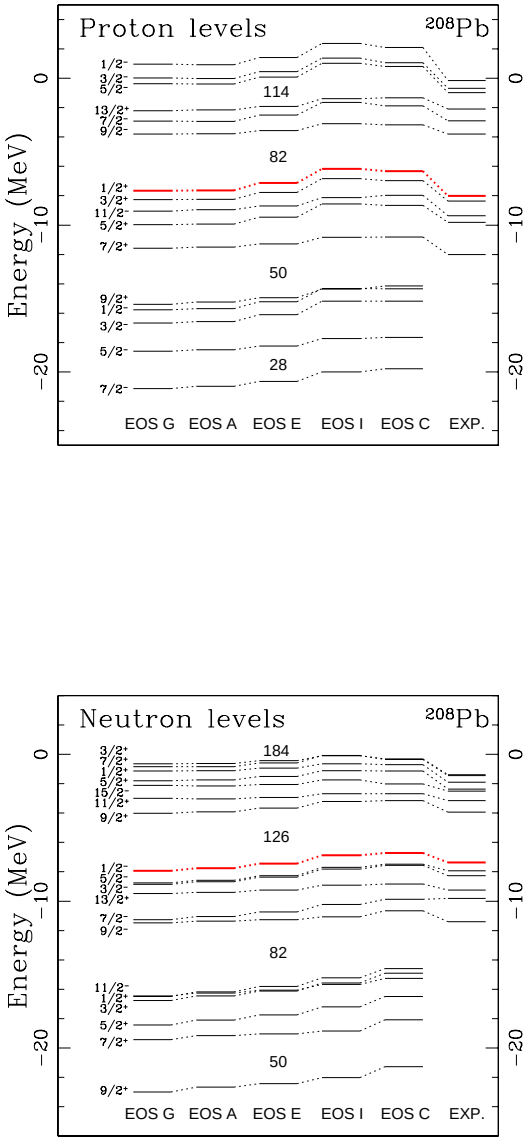

FIG. 1: ^{208}Pb proton (upper) and neutron (lower) single-particle energy levels calculated for various EOS sets. The Fermi levels are drawn in thick red lines. The last column in each panel denotes the experimental data [12].

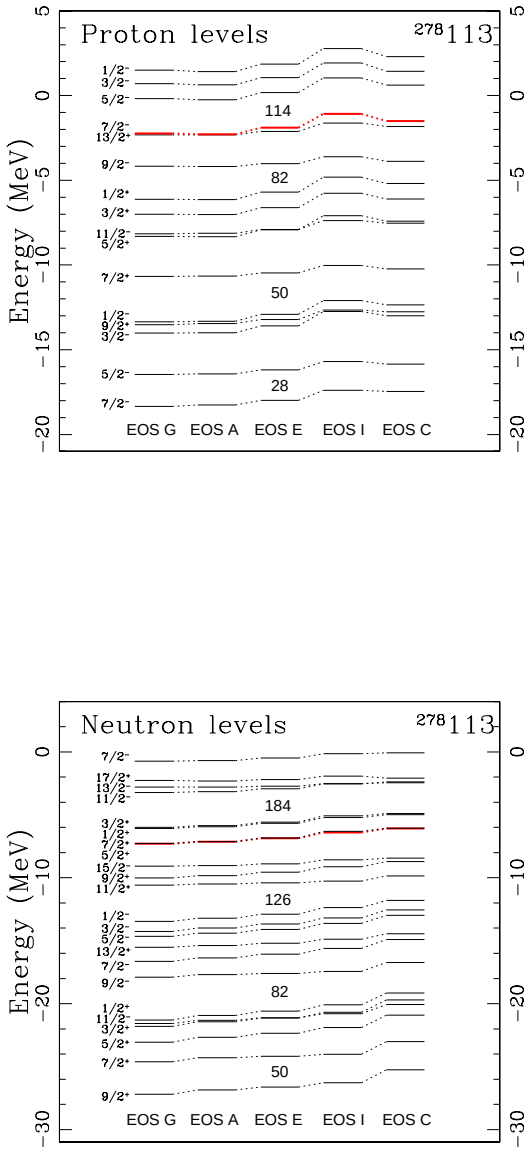

FIG. 2: ^{278}113 proton (upper) and neutron (lower) single-particle energy levels calculated for various EOS sets. The Fermi levels are drawn in thick red lines.

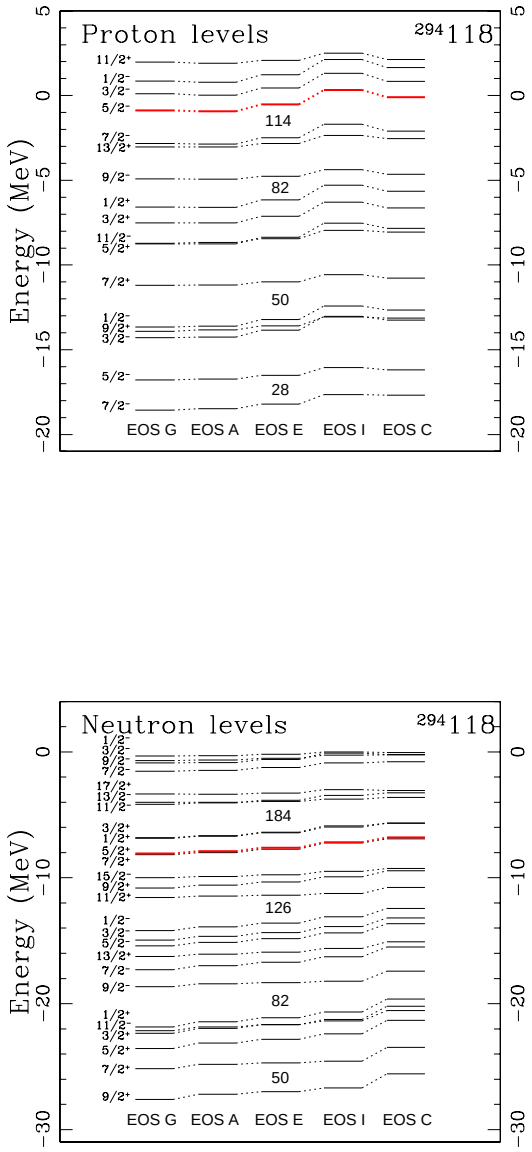

FIG. 3: Same as Fig. 2 in the case of ^{294}118.

island. This is because the fitting to the experimental single-particle energies of ^{208}Pb and the adopted form of the spin-orbit potential (17) severely constrain the location to around $(Z, N) = (114, 184)$, in contrast with, e.g., the previous work based on various mean-field calculations [14]. We also remark that the present analysis neglects possible deformations, which are predicted to be relatively weak for ^{294}118 but significant for ^{278}113 (e.g., Ref. [15]).

In summary, we have constructed the single-particle potential of superheavy nuclei in a manner that is dependent on the EOS of nuclear matter. We have found the sensitivity of the internal proton shell structure to the incompressibility K_0. Deduction of K_0 from data on the breathing modes of stable nuclei ranges 190–315 MeV

TABLE II: The energy gaps (MeV) for various EOS sets.

EOS	G	A	E	I	C
$Z = 28$ (^{208}Pb)	2.54	2.48	2.41	2.27	2.13
$Z = 50$ (^{208}Pb)	3.82	3.74	3.67	3.53	3.34
$N = 50$ (^{208}Pb)	3.56	3.50	3.38	3.17	3.19
$N = 82$ (^{208}Pb)	4.97	4.90	4.79	4.61	4.61
$Z = 28$ (^{278}113)	1.88	1.84	1.79	1.69	1.61
$Z = 50$ (^{278}113)	2.68	2.67	2.46	2.06	2.12
$Z = 82$ (^{278}113)	1.94	1.96	1.69	1.21	1.31
$N = 50$ (^{278}113)	2.58	2.55	2.45	2.26	2.25
$N = 82$ (^{278}113)	3.41	3.25	3.01	2.65	2.43
$N = 126$ (^{278}113)	2.88	2.73	2.48	2.11	1.94
$Z = 28$ (^{294}118)	1.78	1.74	1.69	1.60	1.51
$Z = 50$ (^{294}118)	2.45	2.43	2.33	1.84	1.89
$Z = 82$ (^{294}118)	1.65	1.65	1.39	0.92	1.00
$N = 50$ (^{294}118)	2.43	2.39	2.29	2.12	2.11
$N = 82$ (^{294}118)	3.18	3.01	2.78	2.44	2.21
$N = 126$ (^{294}118)	2.61	2.45	2.21	1.84	1.67

due to large systematic errors [16, 17]. Once uncertainties in K_0 are reduced, a better prediction is expected to be made of the structure of superheavy nuclei. In the present analysis, we have confined ourselves to spherical nuclei. Deformations could play a role in modifying the structure drastically in a far region from the island of stability. The location of the island of stability itself would thus be desired to be specified.

Acknowledgments

We are grateful to H. Koura for useful discussions. This work was supported in part by Grants-in-Aid for Scientific Research on Innovative Areas through No. 24105008 provided by MEXT.

[1] Y. T. Oganessian and K. P. Rykaczewski, Phys. Today **68**, 32 (2015).
[2] K. Oyamatsu and K. Iida, Prog. Theor. Phys. **109**, 631 (2003).
[3] B.-A. Li, À. Ramos, G. Verde, and I. Vidaña, Eur. Phys. J. A **50**, 9 (2014).
[4] K. Oyamatsu and K. Iida, Phys. Rev. C **81**, 054302 (2010).
[5] K. Oyamatsu, K. Iida, and H. Koura, Phys. Rev. C **82**, 027301 (2010).
[6] K. Morita, K. Morimoto, D. Kaji, T. Akiyama, S. Goto, H. Haba, E. Ideguchi, R. Kanungo, K. Katori, H. Koura, H. Kudo, T. Ohnishi, A. Ozawa, T. Suda, K. Sueki, H. Xu, T. Yamaguchi, A. Yoneda, A. Yoshida, and Y. Zhao, J. Phys. Soc. Jpn. **73**, 2593 (2004).
[7] Y. T. Oganessian, J. Phys. G **34**, R165 (2007).
[8] K. Oyamatsu, Nucl. Phys. A **561**, 431 (1993).
[9] J. M. Lattimer, Ann. Rev. Nucl. Part. Sci. **31**, 337 (1981).
[10] B. Friedman and V. R. Pandharipande, Nucl. Phys. A **361**, 502 (1981).
[11] K. Oyamatsu and M. Yamada, Nucl. Phys. A **578**, 181 (1994).
[12] N. Schwierz, I. Wiedenhover, and A. Volya, arXiv:0709.3525.
[13] J. Dudek, Acta Phys. Pol. B **9**, 919 (1978).
[14] K. Rutz, M. Bender, T. Bürvenich, T. Schilling, P.-G. Reinhard, J. A. Maruhn, and W. Greiner, Phys. Rev. C **56**, 238 (1997).
[15] H. Koura, T. Tachibana, M. Uno, and M. Yamada, Prog. Theor. Phys. **113**, 305 (2005).
[16] E. Khan and J. Margueron, Phys. Rev. C **88**, 034319 (2013).
[17] J. R. Stone, N. J. Stone, and S. A. Moszkowski, Phys. Rev. C **89**, 044316 (2014).